Influence of scour depth and type on p–y curves for monopiles in sand under monotonic lateral loading in a geotechnical centrifuge

Chortis, G.; Askarinejad, A.; Prendergast, L. J.; Li, Qiang; Gavin, K.

DOI
10.1016/j.oceaneng.2019.106838

Publication date
2020

Document Version
Final published version

Published in
Ocean Engineering

Citation (APA)
Chortis, G., Askarinejad, A., Prendergast, L. J., Li, Q., & Gavin, K. (2020). Influence of scour depth and type on p–y curves for monopiles in sand under monotonic lateral loading in a geotechnical centrifuge. *Ocean Engineering*, *197*, Article 106838. https://doi.org/10.1016/j.oceaneng.2019.106838

Ocean Engineering 197 (2020) 106838

Contents lists available at ScienceDirect

Ocean Engineering

journal homepage: www.elsevier.com/locate/oceaneng

Influence of scour depth and type on *p–y* curves for monopiles in sand under monotonic lateral loading in a geotechnical centrifuge

G. Chortis [a], A. Askarinejad [a], L.J. Prendergast [b,*], Q. Li [a], K. Gavin [a]

[a] Faculty of Civil Engineering and Geosciences, Delft University of Technology, Building 23, Stevinweg 1 / PO-box 5048, 2628, CN Delft / 2600, GA, Delft, the Netherlands

[b] Department of Civil Engineering, Faculty of Engineering, University of Nottingham, Nottingham, NG7 2RD, United Kingdom

ARTICLE INFO

Keywords:
Offshore monopiles
p-y curves
Centrifuge modelling
Scour

ABSTRACT

The influence of scour on the lateral response of monopile foundations for offshore wind turbines is investigated in this paper. Application of lateral load-displacement (*p-y*) curves to predict the lateral pile behaviour is subject to uncertainty as many of the presently used design approaches have been derived for long, slender piles. These piles, with typical length/diameter ratios (*L/D*) of greater than 10 behave differently compared to rigid monopiles, with *L/D* typically less than 6. In this paper, centrifuge tests are conducted on a monopile model under various scour scenarios and *p-y* curves are derived from strain gauges embedded along the model pile wall. Global scour and two different shapes for local scour holes are studied. Using the piecewise polynomial method for extraction of *p-y* curves from sparsely distributed strain measurements, it is recommended to use a 4th order polynomial for the moment profile to extract soil reaction and a 7th order polynomial for the moment profile to calculate pile deflection. Results indicate that the pile behaviour is significantly influenced by the nature (size, shape) of the scour holes affecting the pile–soil system and suggest that the *p-y* curves should be appropriately modified to account for this behaviour.

1. Introduction

Renewable energy is gaining traction worldwide as technologies improve and political pressure to reduce fossil fuel usage mounts. Offshore wind turbines in particular are becoming significantly more commonplace in Northern and Western Europe. Monopiles are the preferred foundation solution for offshore wind due to ease of fabrication and installation offshore (Byrne et al., 2018). The share of turbines founded on monopiles increased from 75% of offshore turbines in 2012 (Doherty and Gavin, 2012) to 87% in 2018 (Wind Europe, 2018). Monopiles are particularly adept at resisting lateral loads and moments induced by wind, waves and currents, and are also efficient at transferring super-structural dead loads to the foundation soil.

It is well-understood that cylindrical structures founded in soil and subjected to hydraulic actions can lead to local scour hole formation (Sørensen and Ibsen, 2013; Prendergast et al., 2015). In fact, many types of foundations including pile groups and caissons located in deep waters can be adversely affected by scour development (Liang et al., 2019). The magnitude of scour depth that can develop under given flow conditions is an area of ongoing research, and the DNV design code suggests a value of 1.3 times the pile diameter (1.3*D*) be considered in design for both ultimate (ULS) and serviceability limit states (SLS), respectively (Det Norske Veritas, 2007) for monopiles. It should be noted that this design specification is for the case of current-only induced scour erosion. The combined actions of waves, currents and tides in the marine environment leads to a significantly more complex time-varying scour interaction process (Negro et al., 2014; Qi and Gao, 2014). Combining this with the natural process of seabed migration, the overall scour regime affecting a particular wind farm can be very difficult to predict. Difficulties in estimating the scour depth is exacerbated by variabilities between empirical formulae developed for scour depth calculation as investigated by previous researchers (Matutano et al., 2013).

The formation of scour essentially increases the free cantilevered length of a monopile and simultaneously reduces the strength and the stiffness of the soil around the pile due to the lower remaining overburden pressures, potentially compromising the stability of the monopile (Hoffmans and Verheij, 1997; Sumer and Fredsøe, 2012). Several researchers have previously investigated the effect of scour

* Corresponding author.
E-mail addresses: G.Chortis@student.tudelft.nl (G. Chortis), A.Askarinejad@tudelft.nl (A. Askarinejad), luke.prendergast@nottingham.ac.uk (L.J. Prendergast), Q.Li-3@tudelft.nl (Q. Li), K.G.Gavin@tudelft.nl (K. Gavin).

https://doi.org/10.1016/j.oceaneng.2019.106838
Received 30 November 2018; Received in revised form 16 October 2019; Accepted 7 December 2019
Available online 17 January 2020

formation on the lateral response characteristics of piles (Li et al., 2018; Prendergast et al., 2013). Reese et al. (1989) presented an overview of the scour formation process in cohesive soils, focusing on the gap created at the soil-pile interface due to water injection induced by the cyclic loading. They concluded that this gap increases with the number of cycles, leading to a considerable decrease in lateral capacity. Bennett et al. (2009) investigated how scour influenced the response of pile groups supporting Kansas Bridge, and showed that the total lateral capacity was significantly reduced by the scour formation. The bending moment and deflection profiles along the piles were significantly altered before and after scouring. Kishore et al. (2009) performed small-scale laboratory tests at 1 g on PVC and aluminium piles in marine clay with and without scour, under monotonic and cyclic loading. They concluded that the formation of scour led to considerably larger bending moments and pile deflections under a given load. Furthermore, they report a reduction in the ultimate lateral capacity, especially when cyclic loads were applied. Similar trends were observed by Li et al. (2009), who focused on bridge piers in order to study the sensitive scour range, in which the soil-pile system's mechanical properties are highly affected. Liang et al. (2018) investigated the influence of vertical loads on lateral responses of piles under scour in marine clay, where the effects of soil stress history and scour hole geometry were taken into consideration. An analytical model based on the principle of minimum potential energy was developed. The study concludes that scour depth plays the most significant role (among various scour hole dimensions – depth, width and side slope angle) influencing the responses of piles under combined vertical and lateral loading. Mostafa (2012) performed numerical studies of the effects of scour on piles in both sandy and clayey soils for different scour hole geometries. They concluded that the influence of scour is more significant in sands than in clays and that global scour has a larger influence than local scour. Li et al. (2013) investigated the behavior of laterally loaded single piles in clay subjected to scour using numerical methods. They studied the influence of scour hole geometry, and showed that the depth of the scour hole has a larger influence than its width.

The lateral response of a monopile can be modelled using 1D finite-element approaches based on a beam on a nonlinear Winkler foundation (Kampitsis et al., 2013; Yankelevsky et al., 1989). A beam model is used to simulate the pile behaviour and discrete, nonlinear lateral springs distributed along the length of the beam can be used to model the nonlinear lateral soil behaviour. The load-displacement behaviour of these springs can be characterised by *p-y* curves, which correlate the soil pressure *p* at a given point along the pile to the lateral pile deflection *y*. Several *p-y* formulations exist for a range of soil types and these approaches offer designers a means for rapid assessment of lateral pile behaviour with the ease of accounting for soil layering. Several researchers (Matlock, 1970; Reese et al. 1974, 1975; Reese and Welch, 1975; O'Neill and Murchinson, 1983) have developed formulations for *p-y* curves, however the majority of these were derived from load tests performed on piles with large length to diameter (*L/D*) ratios that are relatively flexible when compared to the rigid piles used in the offshore wind sector. Because of their deflected shape, rigid monopiles develop additional components of resistance (Byrne et al., 2019) that are not considered by the commonly adopted hyperbolic sand model, as formulated in the API design code (API, 2007) for flexible piles.

In addition to the ongoing uncertainty with *p-y* approaches commonly adopted in design, the effect of scour on the *p-y* characteristics is not fully understood. Some previous studies such as Lin et al. (2010) have investigated this by performing numerical analyses. Due to the inability of *p-y* curves to account for the 3D geometry of a scour hole, Lin et al. (2010) developed a simplified *p-y* method based on a wedge-type failure, which produced results close to the ones of finite element numerical investigations. The conclusion drawn by their research is that the scour depth is the most crucial factor in diminishing the soil lateral capacity as opposed to the width and the angle of the scour hole. In addition, they compared models where all the soil was removed up to a given scour depth (global scour) with ones where only a wedge of soil was eroded (local scour). The result was an extremely large reduction in the lateral soil capacity for the global case, which was about 50% lower than the equivalent capacity in the local scour case. Qi et al. (2016) performed centrifuge tests on flexible piles subjected to scour. They stated the importance of the scour hole geometry, especially due to the different overburden pressure developed between global (complete removal) and local scour. In the global scour tests, the derived *p-y* curves at the same distance from the new mudline were practically the same, regardless of the scour depth. However, in the local scour cases the overburden pressure led to stiffer responses in the scour-extracted *p-y* curves compared to the global cases for the same equivalent depth. They proposed an effective soil depth that would take into account both scour geometry and overburden pressures. It should be noted though that the piles used in the centrifuge tests had a slenderness ratio (*L/D*) of 11.4 and 35, meaning that they behave as slender piles, very different from the short rigid piles used in wind farms, which typically have a *L/D* of approximately 5.

In this paper, the effect of scour hole type and shape on the derived *p-y* curves of a rigid monopile is investigated through centrifuge testing. Tests are conducted in dry sand conditions for different scour profiles, and the *p-y* curves are derived from embedded strain gauges along the model pile under monotonic lateral loading. Two shapes for local scour holes are adopted to investigate the influence of overburden pressure. These are termed narrow and wide in this study, which refer to the base width of the scour hole. The research highlights some important characteristics of scour on measured *p-y* curves and also provides some insight into the inefficiencies of *p-y* approaches for modelling rigid monopiles.

2. Experimental set-up

2.1. Physical model

In this study, experiments were performed at an enhanced acceleration field of 100 times the Earth's gravity (100 g) using the geotechnical centrifuge at TU Delft (Allersma, 1994). The gravity is limited to a maximum of 100 g to prevent issues with the data-logging system. Fig. 1 shows a schematic and photo of the experimental arrangement. The dimensions of the model pile are chosen so as to model a monopile used for offshore wind, which typically have $L/D < 6$ (Doherty and Gavin, 2012; Prendergast et al., 2015; Sørensen and Ibsen, 2013; LeBlanc et al., 2010). The wall thickness of the model pile is selected based on the similitude between the flexural rigidity (*EI*) of the prototype (p) and the model (m), see Eq. (1).

$$(EI)_p = (EI)_m N^4 \quad (1)$$

where *E* is the Young's modulus of the pile material, *I* is the second moment of area of the cross section of the monopile, and N is the geometrical scaling factor, which is 100 in the analysis in this paper. The minimum pile wall thickness (t_{min}) according to (API, 2007) is shown in Eq. (2)

$$t_{min}\ (\text{mm}) = 6.35 + D/100 \quad (2)$$

From Eq. (2), the thickness of the prototype pile wall should be larger than 24.35 mm. Assuming a steel ($E = 210$ GPa) prototype pile with a wall thickness of 30 mm, the flexural stiffness will be $(EI)_p = 13.7$ GN m^2. Therefore, the flexural stiffness of the model pile should be N^4 times smaller, i.e. $(EI)_m = 0.137$ kN m^2. The model pile is fabricated from aluminium with Young's modulus of 70 GPa, therefore, the thickness of the model pile is required to be ~ 1 mm. The adopted model pile dimensions simulate a rigid, open-ended monopile with an outer diameter of 1.8 m, a wall thickness of 0.03 m, embedment length of 9 m and bending stiffness (*EI*) of 13.7 GN m^2 at prototype scale. It should be noted that the prototype dimensions are smaller than typically observed

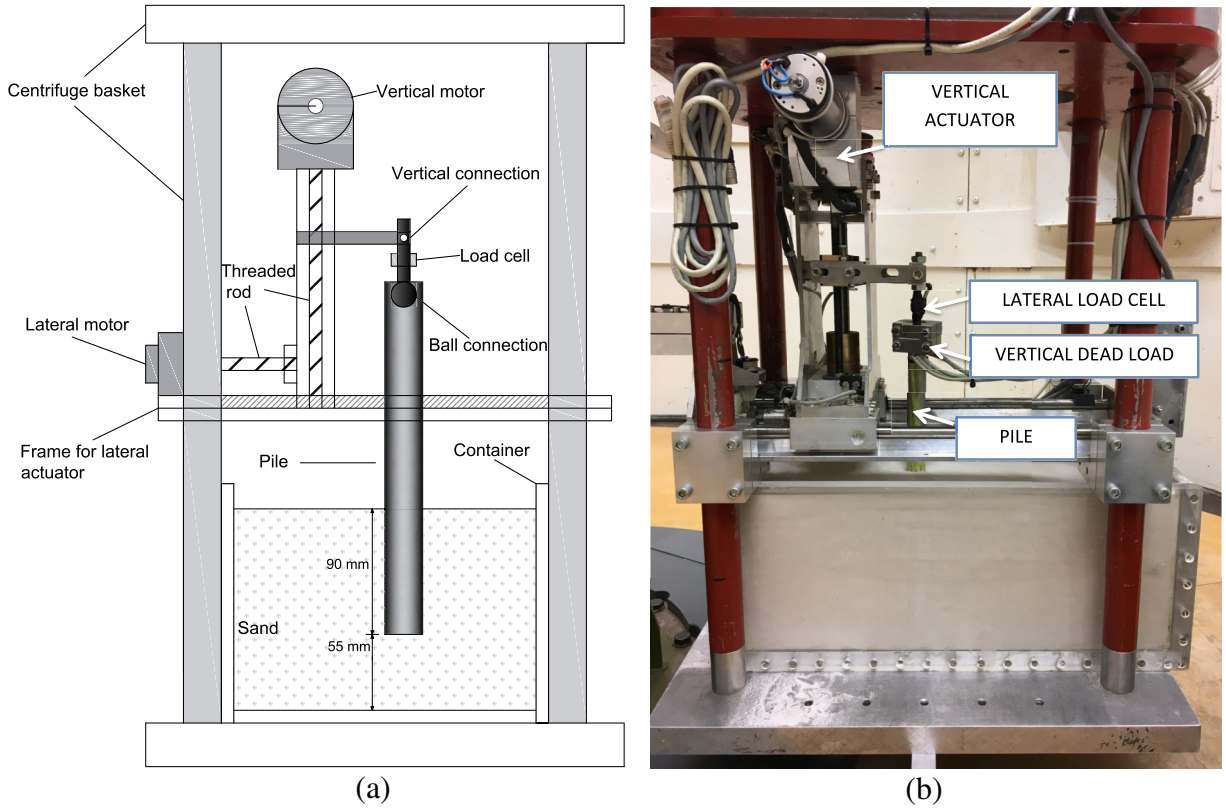

Fig. 1. The 2D actuator and monopile in centrifuge tests (a) Schematic diagram and (b) photo of experimental arrangement.

for offshore monopiles (typical diameters 3–6 m). However, previous research (Byrne et al., 2015) has shown that it is the *L/D*, rather than the pile diameter, that controls the response of piles, so it is more important to maintain a similar *L/D* for comparison to full-scale monopiles. The reason for adopting the smaller diameter in the present case is to avoid issues with model boundary conditions, as discussed in section 2.2, and due to the limiting gravitational acceleration that can safely be used.

Ten pairs of strain gauges are installed along the pile shaft from which the bending moment profile for a given applied load can be derived. These strain gauges are spaced evenly along the embedded length of the pile, see Fig. 2. The gauges are covered with a sealing layer to protect the sensors during testing. This protective layer creates a rough interface between the pile and the sand. It should be noted that only 7 of the 10 installed gauges may be monitored at a given time in

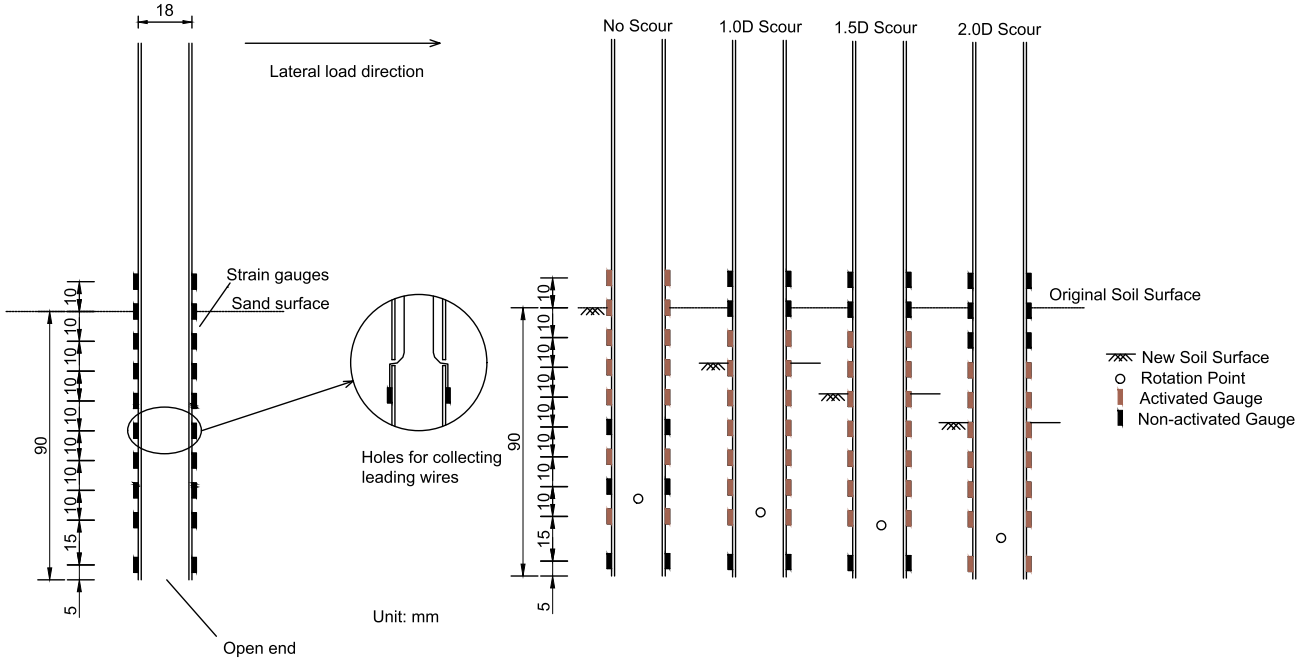

Fig. 2. Schematic of model pile with instrumentation (left) position of strain gauges and (right) strain gauges used for each scour depth.

each test, due to limitations in the number of measurement channels on the data acquisition system. As a result, in each scour case tested in this paper, the data from the most appropriate gauges are logged. For example, in the case where there is no scour, the top most 7 gauge pairs are used as these are the most crucial for producing the *p-y* curves in this case. For the case where a scour hole of 2 pile diameters (2*D*) is implemented, the gauges closest to the original soil surface (i.e. above the scour hole) are omitted, since these are now located above the new soil surface and as such provide no information on the soil reaction for deriving *p-y* curves.

2.2. Soil characteristics and model preparation

The sand used in the centrifuge tests is a uniform fine sand with an average grain size (D_{50}) of 0.11 mm, which results in a pile diameter to average particle size ratio (D/D_{50}) of approximately 160. This is higher than 60, the value suggested by Remaud (1999) for centrifuge testing of piles subjected to lateral loading. The geotechnical characteristics of the sand are summarised in Table 1. All samples have a relative density (D_r) of 80% and are prepared using an air pluviation technique. This technique is carefully controlled to generate a sample with the required relative density so as to ensure consistency between testing. Prior to each test, the sand is placed in a rectangular strong box with dimensions $430 \times 150 \times 180$ mm^3 to a height of 145 mm. The dimensions of the strong box are such so as to minimise potential boundary effects from influencing the results. The ratio of the smallest dimension of the box to the model pile diameter (B/*D*) is 8.3, which is larger than 4 as suggested by Prakasha et al. (2005). The height of the sand is such so as to provide a clearance of more than 3*D* between the pile tip and the base of the box, which is sufficiently large to minimise boundary effects (Prakasha et al., 2005). The model piles are installed in the sand by jacking in place at 1 g in the centre of the strong box prior to each test.

2.3. Local and global scour holes

For the piles tested in this paper, the influence of three different scour hole shapes (global scour and two types of local scour) on the lateral pile behaviour are investigated. Global scour is modelled as the complete removal of a soil layer in the sample, as shown schematically in Fig. 3. This phenomenon can occur as a global action around a whole wind farm site or due to natural seabed migration over a wide area. Local scour is modelled by forming an inverted-circular frustum around the pile as would occur due to changing water-flow characteristics in the direct vicinity of a pile. For local scour, the influence of scour hole shape is investigated by varying the distance from the pile wall to the base of the side slope of the scour hole. This distance, termed W_b (see Fig. 3), is varied between 0 and *D* from the pile. The scour hole with base width $W_b = 0$ is termed *narrow scour* while the scour hole with base width $W_b = D$ is termed *wide scour* in subsequent analyses. The choice of 0 and 1*D* for local narrow and local wide scour is informed from previous studies, which have shown that the behaviour of piles subjected to scour holes with bottom widths larger than 1*D* tend towards the behaviour of piles

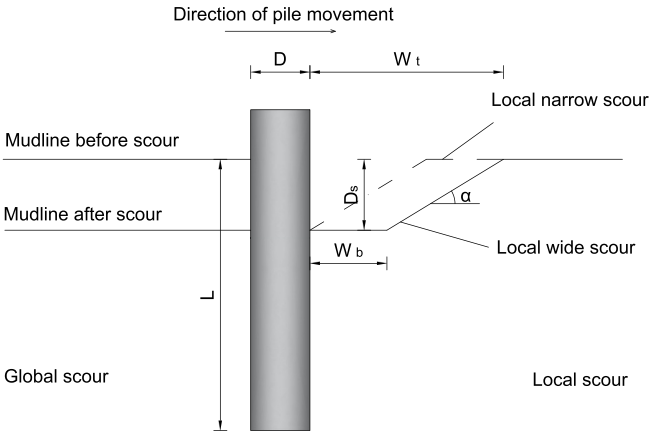

Fig. 3. Schematic showing scour hole shape in centrifuge test.

affected by global scour (Li et al., 2013). In all local scour holes, a side slope angle of $\alpha = 30°$ is adopted, in accordance with Refs. (Hoffmans and Verheij, 1997; Roulund et al., 2005).

To maintain the shape of each modelled scour hole as precisely as possible, rigid plates were fabricated from aluminium with the required geometry for each scour shape. These plates, with varying depths of 1*D*, 1.5*D* and 2*D* (1.8 m, 2.7 m and 3.6 m at prototype scale) had varying base widths of *D* (narrow scour) and 3*D* (wide scour). These plates were used to check the dimensions of scour holes after the sand is removed to ensure consistency. To implement global scour, the whole soil layer from the surface to the required depth was removed after sample preparation. Each scour hole was created prior to installation of the model pile at 1 g and just before accelerating the centrifuge up to 100 g. The programme of testing is presented in section 2.4.

2.4. Testing programme

The testing programme comprises ten tests; one monotonic load test with no scour formation and nine monotonic load tests with three different scour types and three scour depths. The test programme is summarised in Table 2. For each test, the lateral load is applied 1 m below the pile head. The horizontal actuator pushes a ball-joint placed within the pile head at a constant displacement rate of 0.01 mm/s. The inner pile surface is covered with a layer of Teflon to reduce friction between the ball and the pile. This approach aims to minimise any rotational fixity at the pile head that might be imposed by the actuator to remain in keeping with the free head condition of an offshore monopile. The lateral pile displacement is measured at the same location where the load is applied and the measurement accuracy is of the order of 3×10^{-5} mm (at model scale). A vertical load equating to 3 MN at prototype scale is imposed by attaching steel blocks to the top of the pile, which simulates a typical vertical load imposed on a wind turbine pile due to the weight of the superstructure (Prendergast et al., 2018).

Table 1
Geotechnical properties of the sand used in the experiments (De Jager et al., 2017).

Property	Value
Soil Classification Based on USCS[a]	SP (Poorly Graded Sand)
Median Particle Size, D_{50} (mm)	0.11
Curvature Coefficient, C_C	1.24
Uniformity Coefficient, C_U	1.55
Specific Gravity, G_S	2.67
Maximum Void Ratio, e_{max}	1.07
Minimum Void Ratio, e_{min}	0.64
Internal Friction Angle, ϕ	34°

[a] Unified Soil Classification System (USCS) (ASTM, 2017).

Table 2
Programme of centrifuge tests.

Test name	Scour type	Scour depth
Pile-1	No scour	–
Pile-2	Global scour	1.0*D*
Pile-3	Global scour	1.5*D*
Pile-4	Global scour	2.0*D*
Pile-5	Local wide scour	1.0*D*
Pile-6	Local wide scour	1.5*D*
Pile-7	Local wide scour	2.0*D*
Pile-8	Local narrow scour	1.0*D*
Pile-9	Local narrow scour	1.5*D*
Pile-10	Local narrow scour	2.0*D*

3. Analysis

The load-displacement responses measured at the point of application of the lateral load and the bending moment profiles derived from the strain gauges along the embedded pile for a given load magnitude are obtained. The strain gauges are used to ultimately derive *p-y* curves. In tests of this nature, Ultimate Limit State (ULS) failure for a pile is defined as occurring when a lateral pile displacement of 0.1*D* at the soil surface is exceeded. For the tests conducted in this paper, ULS is defined to be a lateral pile displacement of 0.60 m (0.3*D*) at the connection point of the monopile and the actuator (1 m below the pile head) to enable the derivation of *p-y* curves over a large strain range.

3.1. Load-displacement curves and bending moments along the pile

The load-displacement behaviour, at the level of the ball connection point, under different scour depths is shown in Fig. 4. For this analysis, the results of the *local wide scour* cases are shown (see Table 2 and Fig. 3). The increase in the depth of scour around the pile decreases the available soil capacity resulting in lower lateral resistance for a given displacement. At ULS (0.3*D* at the connection point in this case), the reduction in mobilized soil resistance is evident, whereby the unscoured resistance is approximately 400 kN and the resistance at 2*D* scour is 50% of this value, at approximately 200 kN. The lateral soil resistance is governed both by the length of the embedded pile and the effective stress level in the soil surrounding the pile. Increasing the scour depth has the dual effect of decreasing the embedded length of the pile as well as reducing the effective stress in the remaining soil, resulting in lower resistance under applied loading.

Under a given applied load, the strains measured along the pile shaft can be used to derive the bending moment profile. Bending moments are derived from bending strain measurements using Eq. (3).

$$M(z) = EI\rho(z) \tag{3}$$

where E is the Young's modulus of the pile material (N/m^2), I is the cross-sectional moment of inertia of the pile (m^4) and $\rho(z)$ is the curvature at a given applied load, obtained as the ratio between the difference in measured compressive and tensile strains to the gauge lever arm (pile radius) at a given depth z. Fig. 5 shows the pile bending moment profiles under an applied load of 100 kN for zero scour and three depths of local wide scour. The bending moments at various points along the pile are lower in the no scour case compared to the cases with scour around the monopile. This observation implies that the pile structure encounters higher stresses in the case of scour. This mechanism can be attributed to the reduced pile embedment under scour, and the resulting reduction in soil-pile contact area, which requires higher stresses to develop in order for equilibrium to be achieved in the system. Moreover, the location of the peak bending moment also occurs at lower elevations under scour than in the absence of scour.

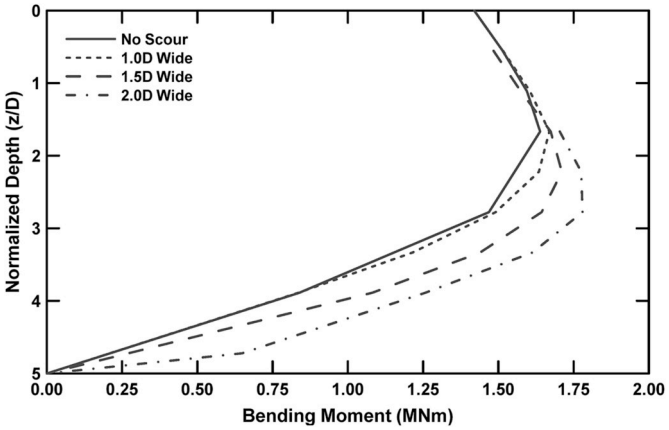

Fig. 5. Bending moment profile under increasing wide local scour at a constant applied lateral load of 100 kN.

Figs. 4 and 5 show the results of increasing scour around the pile for a given scour type, namely *local wide scour*. Fig. 6 shows the load-displacement response at the ball connection point for the maximum scour condition (2*D*) for all three scour types, *local narrow*, *local wide* and *global scour*. The data show that the different scour types result in differences in the load-displacement behavior. Relative to the no scour case, the pile response becomes progressively weaker under *local narrow*, *local wide* and *global scour*, at the same scour depth magnitude of 2*D*. This result suggests a sensitivity to the differences in the overburden pressures around the pile for each scour case. The local scour cases offer higher overburden pressures in the remaining soil than global scour (due to the fact that only a frustum-shaped volume of soil is removed and not the entire soil layer), leading to higher lateral soil resistance. Of note is that local narrow and local wide scour also exhibit this sensitivity to differences in the overburden between these two scour hole shapes, implying that the shape of a scour hole should be considered more closely.

Fig. 7 presents the bending moment profiles for an applied lateral load of 100 kN for the three scour types, at a scour depth of 2*D*. Relative to the no scour condition, the narrow scour type is the most favourable in the terms of soil resistance, while the global and the local wide scour are the most critical cases. The distinction between the latter two cases is not really clear, as the moment profiles have been extracted for a lateral load of 100 kN (a load below ULS). However, at this load magnitude, the displacement of the pile is relatively small, as can be seen by the load-

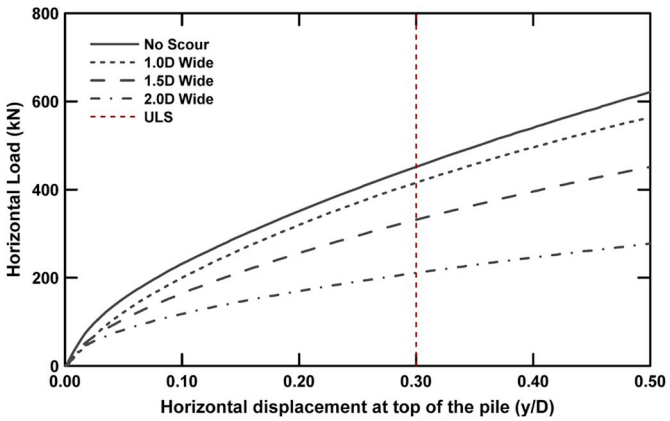

Fig. 4. Lateral load-displacement response under increasing scour depth for the case of wide local scour.

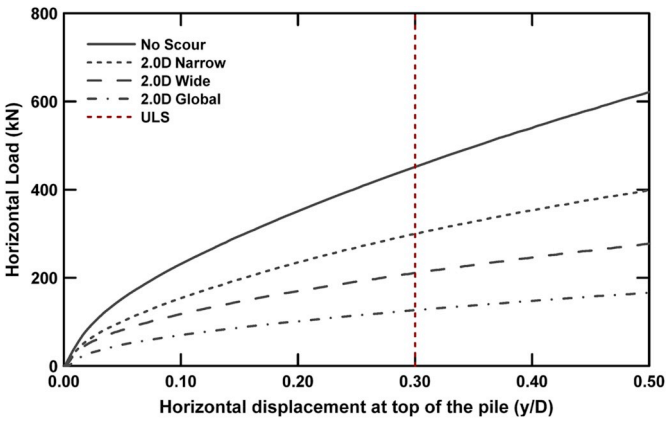

Fig. 6. Lateral load-displacement response under different scour types at constant depth.

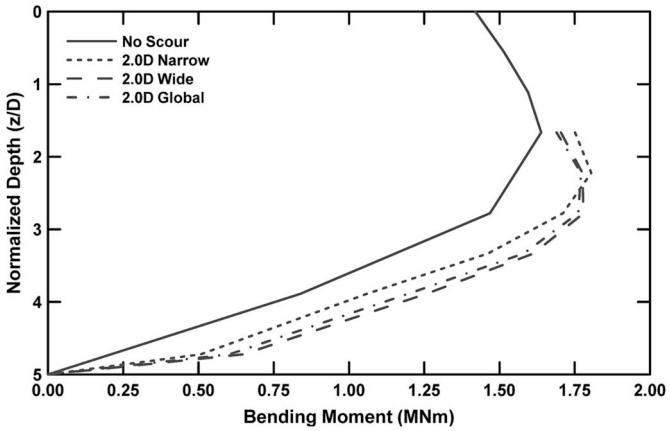

Fig. 7. Bending moment profile under different scour types at a constant horizontal load of 100 kN.

displacement curves in Fig. 6, leading to minor differences in the bending moment profiles. However, for larger displacements, the local wide scour deviates away from the global case and provides intermediate results between the narrow and global case. It is noteworthy that the response under local wide scour will depend highly on the length of W_b, as this parameter defines whether the behavior is closer to local narrow scour or global scour.

3.2. Effect of scour on derived p-y curves

3.2.1. Deriving p-y curves from experimental measurements

Soil reaction-lateral displacement (*p-y*) curves at various points along a pile can be derived from a bending moment distribution along the pile, which can be obtained from strain gauges. A bending moment profile derived using strain gauges is discrete in the sense that one obtains values for the bending moment only at the location of a given strain gauge. In order to derive *p-y* curves at any point of choosing, a continuous profile for the bending distribution is required (Xue et al., 2016). To achieve this, a polynomial curve may be fitted to the discrete bending moment points to estimate a continuous moment profile. The choice of fitted curve, which is studied below, should aim to minimise the error between the discrete bending moment points and the values of the continuous curve at these locations, as these errors affect the quality of the subsequently derived *p-y* curves. The fundamental premise of deriving *p-y* data is as follows: The soil reaction p may be derived as the second derivative of the bending moment M, with respect to depth (z), see Eq. (4). The lateral deflection (y) for a given bending moment may be obtained by integrating the bending moment profile twice, see Eq. (5).

$$p = \frac{\mathrm{d}^2 M}{\mathrm{d}z^2} \tag{4}$$

$$y = \iint \frac{M}{E_\mathrm{p} I_\mathrm{p}} \mathrm{d}z \mathrm{d}z \tag{5}$$

The double integration of discrete data points (the individual moments derived from the strain gauges using Eq. (3)) is favourable in terms of minimizing the measurement errors by the strain gauges. For this reason, numerical errors are negligible when calculating the pile deflection y in Eq. (5). Hajialilue-Bonab et al. (2014) state that odd-degree polynomials used for fitting the moment profile to discrete points are usually more accurate than even-degree polynomials, during the double-integration procedure to calculate the pile deflection y. Contrary to the favourable integration procedure, double differentiation of the discrete data points tends to exacerbate existing measurement errors and thus leads to difficulties in the accurate derivation of soil pressure p. Piecewise Polynomial Curve Fitting (Dunnavant, 1986), High Order Global Polynomial Curve Fitting (Reese and Welch, 1975; Wilson, 1998), Weighted Residuals Method (Wilson, 1998) and Cubic Spline Curve Fitting (Mezazigh and Levacher, 1998) are all methods suggested for deriving the soil pressure p with the minimum error possible. Yang and Liang (2007) evaluated the performance of these methods based on full-scale tests where they compared the curves derived by measurements to ones generated by 1D software applications such as COM624P (Wang and Reese, 1991) or its commercial version L-Pile (ENSOFT INC, 2018). They concluded that the piecewise polynomial approach was the most accurate method, especially for relatively sparse strain measurements, which is the case in the present study.

The piecewise polynomial curve-fitting method (Yang and Liang, 2007) was adopted for the calculation of soil pressure p in this paper. A minor modification was adopted in the present case, namely that a fourth-order polynomial was used instead of a third-order one that was suggested by Dunnavant (1986) & Yang and Liang (2007). This choice was determined by the sparse distribution of the gauges near the bottom of the pile. Specifically, if a third-order polynomial is differentiated twice, it produces a linear expression for the soil pressure distribution. This procedure can be effective only if the gauges are densely spaced, as the consecutive linear expressions and hence the linear soil pressure distribution are applied only to small parts of the pile, and therefore in total the actual curved shape of the soil pressure distribution can be captured. In this series of tests however, the gauges are not spaced with sufficient density, especially near the bottom of the pile, meaning that a linear expression would be applied over too large a portion of the pile length. On the contrary, a fourth-order polynomial differentiated twice produces a second-order equation, which can simulate a non-linear pressure distribution. This detail proved to be important in capturing a more accurate pressure response, at the top and the bottom of the pile, from trials undertaken in this study. Note also that the odd-degree polynomials are considered to be more accurate for the extraction of the pile deflection (Hajialilue-Bonab et al., 2014), but the same claim is not made in the literature for the extraction of soil pressure. The approach adopted in the present paper is described as follows: An n-degree polynomial is fitted to five successive moment data points, derived from the strain gauge data, using a least-squares approach. This polynomial expression is then differentiated twice to derive the soil response p, evaluated at the central data point (of each set of five). The soil pressure response for the uppermost and lowermost three points are obtained from the polynomials fitted to the highest and lowest data points, respectively (Fig. 8, left). For this reason, a third order polynomial when differentiated twice gives a straight line at the top and at the bottom of the pile (unless there are many strain gauges). In this study, a fourth-order polynomial proved to be more suitable for the upper and lower part of the pile, as discussed above.

The lateral deflection of the pile y at discrete locations was calculated by integrating a seventh-order polynomial for the bending moment profile twice (Fig. 8, right) as shown in Eq. (4). Knowledge of two integration constants C_1 and C_2 are required for this procedure, taken as the boundary conditions. C_1 was calculated using the measured displacement at the level of the ball connection (1 m below the pile head at prototype scale). C_2 was determined by making the assumption that zero deflection takes place at the point of zero lateral resistance (point of rotation of the pile), as proposed by Wang and Qi (2008). While this location may be inferred from the derived *p*-profile, this is subject to uncertainty due to errors related to the sparsity of strain measurements, the choice of adopted polynomial order, and the tendency for errors to be exacerbated in the double differentiation process. For this reason, and to ensure as accurate a deflection profile as possible, it should additionally be informed from another source. For the analysis in this paper, a numerical model of the test arrangement was created to inform on this second required boundary condition. The Finite Element (FE) software PLAXIS (Brinkgreve et al., 2016) was used to develop a model of the pile for this purpose, and is described herein.

A 3D FE model of the test pile at prototype scale was developed, see Fig. 9. The purpose of conducting these analyses was to make a

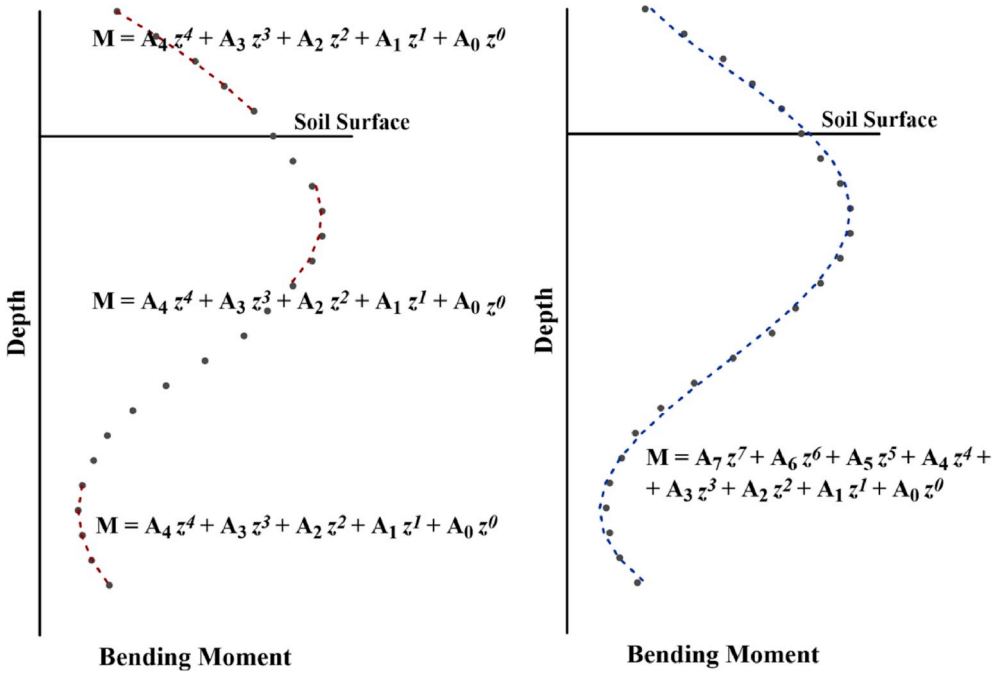

Fig. 8. Schematic illustration of the procedure for extracting the soil pressures from the bending moment profile.

scientifically informed assumption for the depth of the rotation point (zero soil pressure nominally) to be used as the second integration constant in the *p-y* derivation procedure. The geometry of the model is the same as that of the prototype of the centrifuge tests. Due to the scale of the strong box, boundary effects may be present in the analyses so effort was made to ensure the same boundary effects were implemented in the numerical model. A vertical dead load of 3 MN was simulated using a distributed load at the pile top. A Hypoplastic constitutive model for the soil was adopted (Niemunis and Herle, 1997; von Wolffersdorff, 1996) and the soil parameters were calibrated based on element tests. The implemented parameters for the von Wolffersdorff (von Wolffersdorff, 1996) model with the addition of the intergranular strain concept (Niemunis and Herle, 1997) are presented in Table 3. A series of FE simulations were undertaken for cases where no scour affects the pile and where scour equating to the three depths and types from the centrifuge testing were considered. In each simulation, the pile was subjected to a prescribed displacement (at the same displacement

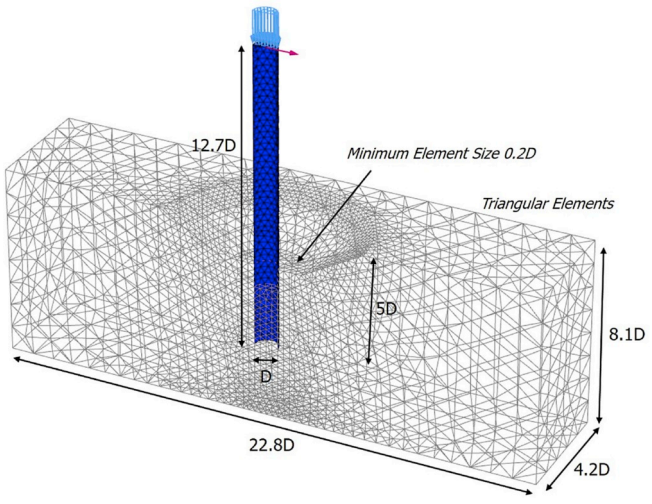

Fig. 9. PLAXIS model that simulates the centrifuge test for a typical wide scour case.

Table 3
Hypoplastic model parameters after the calibration of the PLAXIS 3D model.

von Wolffersdorff's hypoplastic model parameters							
ϕ_c	h_s	n	e_{d0}	e_{c0}	e_{i0}	α	β
34	4200 MPa	0.15	0.640	1.070	1.280	0.07	0.75
Intergranular Strain Concept							
m_R	m_T	R_{max}	β_r	χ			
6.9	5.0	0.0001	0.3	1.0			

magnitudes as in the centrifuge tests at prototype scale) at its top, which corresponded to the level of the ball connection in the centrifuge set-up. The deflection of the pile along its length was measured under these varying lateral displacements. From these simulations, the rotation point was shown to occur at a depth of approximately 70% of the current embedded pile length and remained constant for each scour case, independent of the magnitude of the lateral displacement. In Fig. 10 a characteristic set of the aforementioned analyses is shown, for the no-scour case and for three different scour depths (1*D*, 1.5*D* & 2*D*) of the local wide scour case, where the ratio of rotation point depth to the new embedded pile length (after scour) is approximately 0.7. This location is used as the second 'known' boundary condition for the lateral displacement derivation. Note also as an aside that the rigid behavior of the pile is clearly illustrated in the graphs of Fig. 10.

3.2.2. Derived p-y curves for zero scour case

Based on the aforementioned procedure, the evolution of the pile deflection and the soil pressure distribution for the no-scour case have been calculated in Figs. 11 and 12, respectively from the centrifuge tests. This analysis is undertaken for constant displacement increments of 0.10 m at the connection point between the pile and actuator. The rigid behaviour of the pile is clearly evident in Fig. 11, where the pile rotates as a rigid body around the assumed rotation point at 70% of the embedded pile length (as informed from the numerical analyses). This response differs from that of a long slender pile, such as those for which the industry-standard *p-y* curves from the API method (API, 2007) have been extracted (Murchison and O'Neill, 1984). The rigid piles develop a 'toe-kick' (Achmus, 2010) at the pile toe, which mobilises high soil

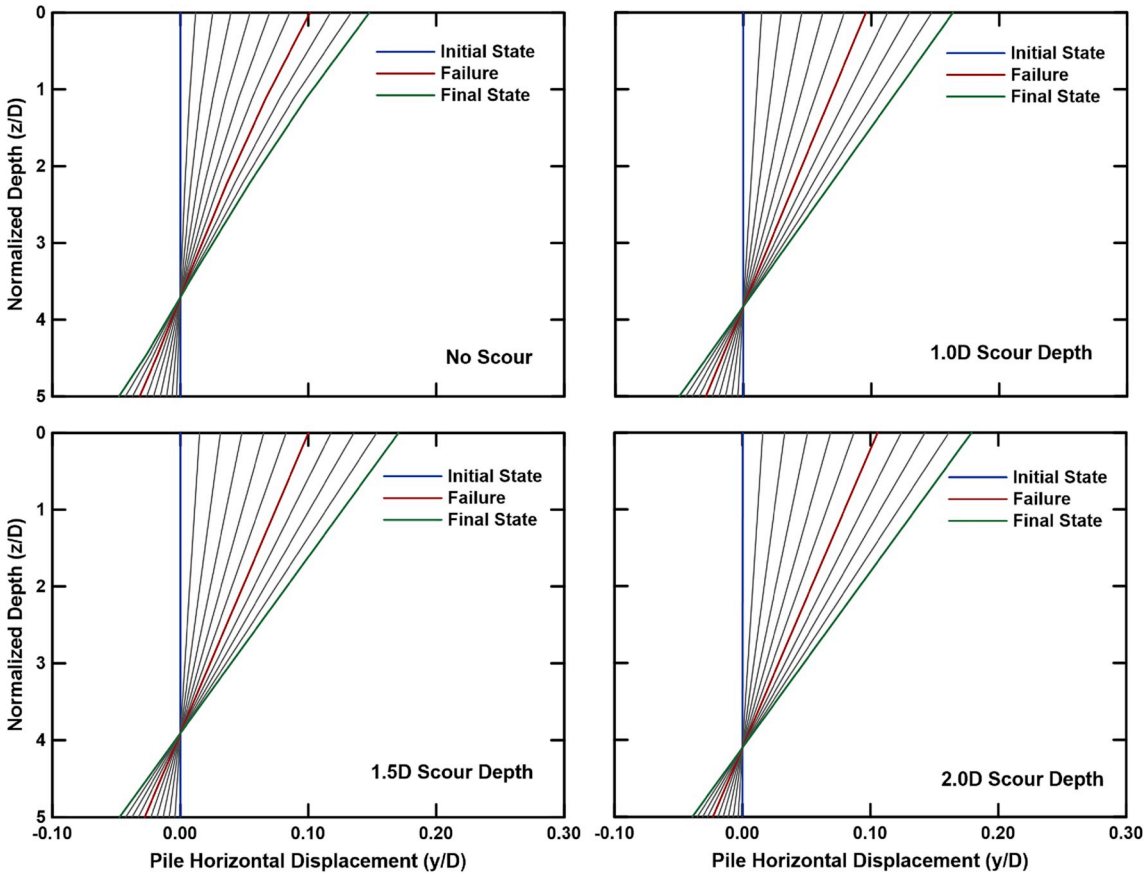

Fig. 10. Evolution of the pile deflection for the no-scour case and the three scour depths (1*D*, 1.5*D* & 2*D*) for a constant interval of 0.10 m pile displacement at the connection point in the PLAXIS model.

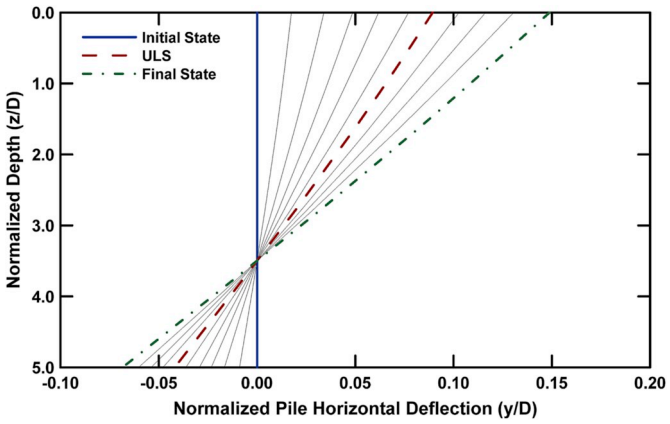

Fig. 11. Evolution of the pile deflection for the no scour case.

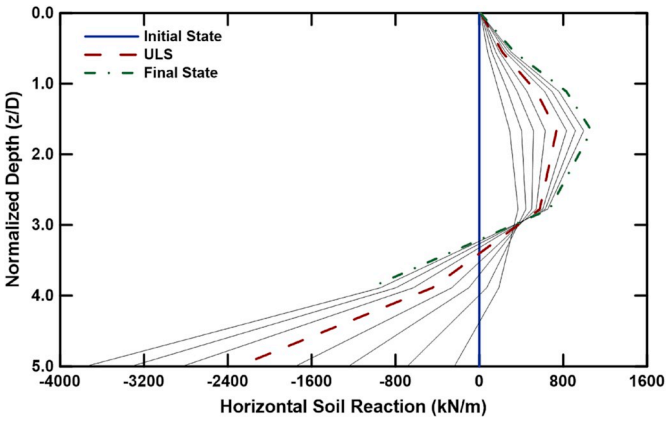

Fig. 12. Evolution of the soil pressures for the no scour case.

resistance. In Fig. 12, high soil pressures are observed close to the pile toe. Fig. 12 also exhibits some soil pressure in the region of the point of rotation, where these should be zero. This error occurs as there are few strain gauges below the rotation point, which leads to inevitable errors in the fitted data for the moment profile. Moreover, the double-differentiation procedure to derive soil pressure from the bending moment profile exacerbates measurement errors, as previously discussed. This could be improved with the use of a higher density of strain gauges, to provide more continuous strain profiles and thus mitigate issues related to curve-fitting of the moment profile. For the case in the present study, the limitation is due to the available hardware. In both Figs. 11 and 12, ULS refers to the displacement of 0.3*D* at 1 m below the pile head (ball connection level) as previously defined.

Using the data in Figs. 11 and 12, the *p-y* curves for the no-scour case have been extracted as shown in Fig. 13. For comparison, the *p-y* curves have also been constructed using the API method (API, 2007) in Fig. 13. The sign of the soil reaction is defined by the single rotation point (see Fig. 11), i.e. whether the soil on the right-hand or left-hand side of the pile is providing the resistance at a given depth. The initial stiffness of the soil increases with depth, as observed by the increasing angle of the initial portion of the derived *p-y* curves. The soil resistance increases with depth, since for a given displacement, the equivalent (absolute) soil pressure is largest for the case $z/D = 3.90$, with the $z/D = 2.78$, 1.67, 1.10 & 0.55 decreasing accordingly. Note the length of a given *p-y* curve

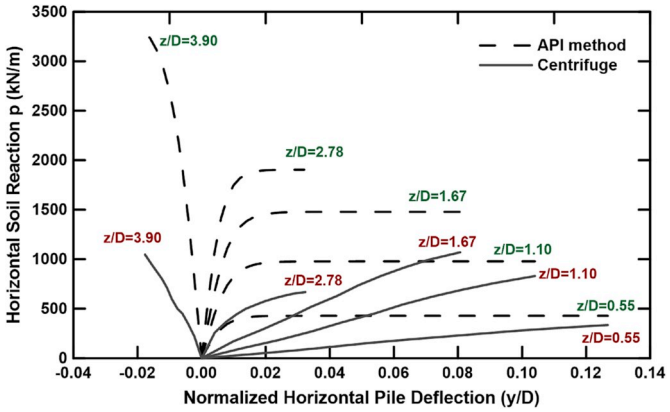

Fig. 13. *p-y* curves for the no scour case for various depths.

is limited by the displacement of the pile at that location, which explains the shorter curves at z/*D* = 2.78 and 3.90 (nearer assumed rotation point). The increase of the soil capacity with depth indicates that in order to reach equilibrium, the rotation point must be closer to the tip of the pile, as observed in Fig. 11 and 12. Above the rotation point, the largest soil resistance occurs at a depth z/*D* = 1.67, which is also the location of the highest bending moment. Relative to the *p-y* curves derived in this paper, the API approach overestimates the soil resistance. Moreover, the API initial stiffness is high and the ultimate resistance is in some cases more than twice that measured from the centrifuge test data. This difference between the API and the derived curves is most likely attributable to the rigidity of the test pile, as the API method is more applicable to long, slender piles. Note also, a slender pile tends to have little to no pile tip deflection whereas a rigid pile can have significant deflection at this location.

3.2.3. *Effect of scour on the characteristics of the p-y curves*

The effect of scour depth and type on the characteristics of the derived *p-y* curves is investigated in this section. *p-y* curves for the piles subjected to different scour types (local narrow, local wide, and global) are derived for three different scour depths; namely 1*D*, 1.5*D*, and 2*D* in Figs. 14, 15 and 16, respectively. In each graph, the *p-y* curves are illustrated for the same scour depth, for all three scour types. Note, the curves at normalized depths z = 1.67*D*, z = 2.2*D*, z = 2.78*D*, z = 3.33*D* occur above the pile rotation point, while the curve z = 4.7*D* occurs below it. The curve at z = 3.9*D* is close to the rotation point, hence limited data is available due to the small lateral deformations at this point. For each plot, only certain curves are produced due to the limited number of strain gauges available in each case (only 7 of the 10 gauges may be logged simultaneously on the system). In Figs. 14 and 15, the

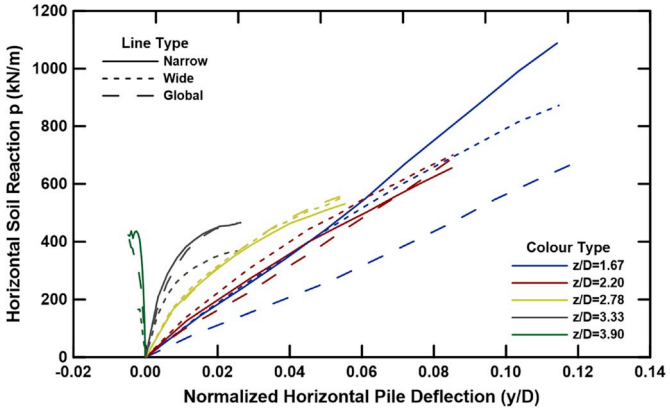

Fig. 14. *p-y* curves for the 1*D* scour depth case at various depths for a narrow, wide and global scour type.

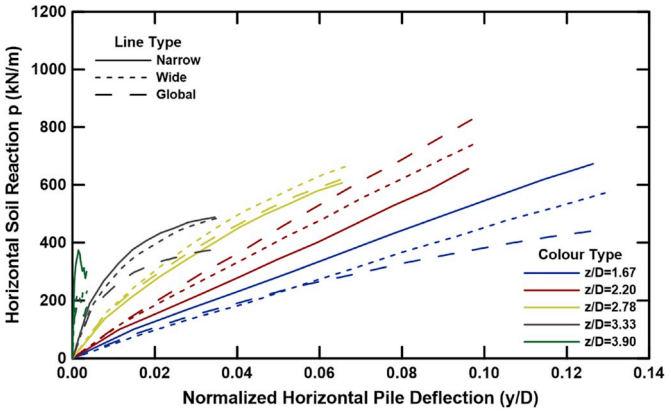

Fig. 15. *p-y* curves for the 1.5*D* scour depth case at various depths for a narrow, wide and global scour type.

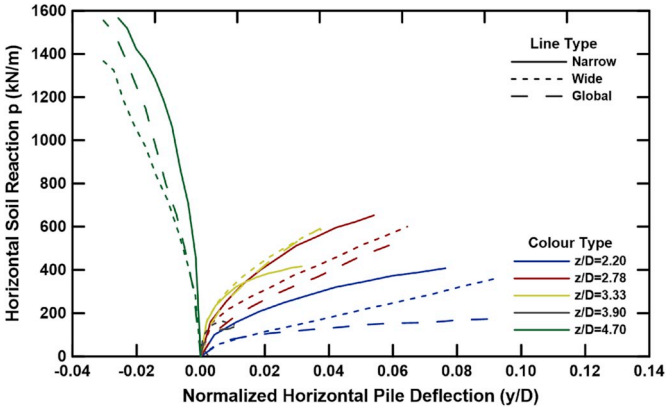

Fig. 16. *p-y* curves for the 2*D* scour depth case at various depths for a narrow, wide and global scour type.

curve at z/*D* = 4.7 is omitted and in Fig. 16, the curve at z/*D* = 1.67 is omitted.

The results in each plot show that the *p-y* curves at shallower depths (z = 1.67*D*, z = 2.2*D*) are considerably affected by the scour type. At z = 1.67*D* in Figs. 14 and 15, the response of the local narrow scour case is stiffer than those of the local wide and global scour cases, as the overburden pressure is almost the same as the no scour case, Fig. 13 (only a small frustum of soil has been removed around the pile for the local narrow scour scenario). At larger depths, while still above the rotation point in all plots (z = 2.78*D*, z = 3.33*D*) the *p-y* curves for all three scour types begin to converge, implying that the effect of scour type is not so important at larger depths. Some small differences still exist between these curves, as in Fig. 14 for the depth of z = 3.33*D*, which may be attributable to experimental error in the calculation of the *p-y* curves as different tests were conducted in each case. Observing the curves at z = 4.7*D* (below the rotation point) in Fig. 16 a very stiff response occurs.

The conclusion that may be drawn by Fig. 14, 15 and 16 is that the scour type highly affects the *p-y* curves at the shallower depths, while as the depth becomes larger this effect becomes less severe. The geometry of the local scour hole, whether wide or narrow in these experiments, influences the *p-y* curves, leading to a ≈20% reduction in ultimate resistance for the local wide scour case compared to the local narrow case. Moreover, the *p-y* curves for the global scour cases, in the shallow depths can be smaller in a range of 20% up to even 40% from the ones of the local scour cases.

3.2.4. *Validation of derived p-y curves*

In this section, the *p-y* curves derived from the centrifuge testing are

inputted into a 1-dimensional (1D) numerical finite-difference solver to ascertain if the model can predict the pile load-displacement curve and bending moment distribution as was measured during the experimental tests. The purpose of this is to validate the derived *p-y* curves. The software L-Pile was used to perform this analysis. L-Pile is a 1D solver, which simulates the lateral pile response using non-linear springs. It is possible to specify either industry standard curves such as API sand, or to input user-specific curves, which makes this software ideal for the purpose of benchmarking the experimental data in this paper. The *p-y* curves calculated from the centrifuge test results were used as input parameters to the L-Pile software, with the boundary conditions (load and moment applied to the pile) at the soil surface level. The pile head load-displacement curves from the centrifuge tests and the L-Pile analysis were compared. Furthermore, the bending moment profiles produced by L-Pile were compared with the ones derived from the strain gauge data in the centrifuge tests. An example of this process is presented herein. Fig. 17(a) shows the *p-y* curves derived at various depths along the pile for the case of 2*D* global scour. These *p-y* curves are inputted into L-Pile, and the equivalent bending moment distribution was calculated under three lateral loads (50, 100, 150 kN). These bending moment profiles produced by L-Pile were then compared with the bending moments derived from the strain gauge measurements for the same lateral loads for the 2*D* global scour case. A scour case with a depth of 2*D* has been chosen for this comparison because of the availability of strain gauge measurements below the rotation point.

In the upper part of the pile (around 50% of the embedded pile length) there is close agreement between the L-Pile results and the experimental data, indicating that the derived *p-y* curves are correctly calculated from the data. However, at the bottom of the pile, the centrifuge test results show higher values of bending moment compared to those calculated using L-Pile. This deviation is most likely due to the high horizontal passive soil pressure and shear stresses mobilized at the tip of laterally-loaded rigid piles in the experiment, which result in the potential existence of large bending moments above the base. L-Pile does not take into account the possible shear force developed in the annular part of the pile tip and hence this extra resistance is not included. This is potentially the reason why the L-Pile produced curves exhibit a smaller magnitude relative to the experimental curves close to the pile toe. Fig. 18 shows the measured pile head load-displacement curve compared against the curve extracted from L-Pile for the same case of 2*D* global scour. A reasonably good match is obtained, with some under-prediction in the capacity being observed in the L-Pile curves. This under-prediction is sensible as the L-Pile analysis omits the presence of potential base shear forces, which would increase the lateral capacity.

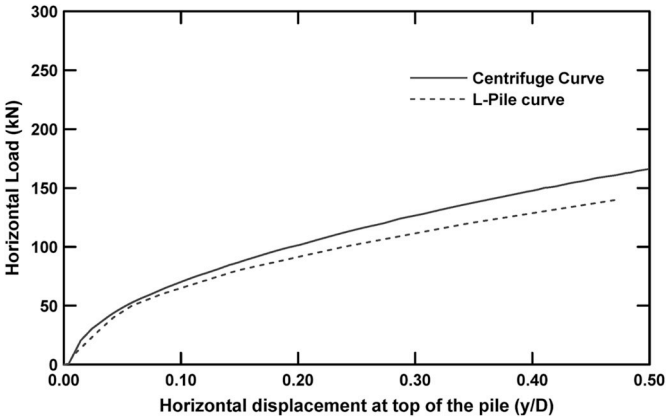

Fig. 18. Pile head load-displacement curves from the centrifuge testing and L-Pile for the case of 2*D* global scour.

Overall, the extracted *p-y* curves from the centrifuge tests are reasonably well validated by the L-Pile software and moreover this analysis highlights the disparity in predictions that can occur for rigid monopiles.

3.2.5. Recommendations

The effect of the scour formation on *p-y* curves is case sensitive at relatively shallow depths. Global and local scour lead to *p-y* curves with different ultimate capacity, which may be up to 40% lower for the global case as compared to the no scour case. Similarly, the 'catch-all' term "local-scour" seems to be insufficient, since the geometry of the local scour hole highly influences the response characteristics, producing *p-y* curves that can differ by up to 20% in ultimate capacity for the conditions tested in this study. Therefore, taking into account the difficulty in accurately predicting the scour formation (depth and type) it is highly recommended that a full-range analysis of scour be performed in each relevant project. Scour depth and type should be investigated in such an analysis, by focusing on the geometry of the scour hole and overburden pressure considerations, for local scour cases. Local narrow scour and global scour are the two extremes, while the local wide case is an intermediate scenario, hence a valid analysis should contain at least these scenarios to make sure a given structure will be adequately designed against scour occurrence.

It is recommended that *p-y* curves used by industry should be updated to have a better application to rigid monopiles. Approaches to

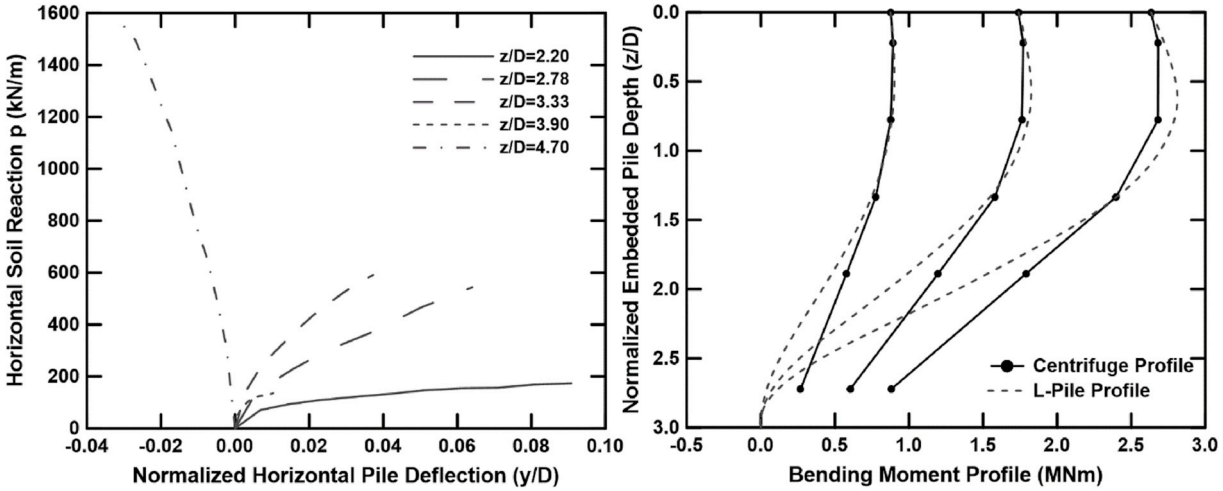

Fig. 17. (a) *p-y* curves for the 2*D* global scour case for various depths (b) Equivalent bending moment profile from centrifuge and L-Pile for three different horizontal loads.

incorporate additional resistance components due to shear force mobilized at the base and shear stresses mobilized along the pile during rotation are discussed in Burd et al. (2017).

4. Conclusions

This paper presents a series of centrifuge tests for a monopile subjected to lateral loads for different scour depths and types. A method is presented for deriving *p-y* curves for rigid piles and its applicability is evaluated. The effect of scour type on the derived *p-y* curves is investigated. The findings of this paper are summarised as follows:

- The Piecewise Polynomial approach is a reasonably valid method for fitting a discrete bending moment profile and used in the subsequent derivation of soil pressure developed along the length of the monopile. For sparsely distributed gauges, a 4th order curve performs well. For extracting the deflection of the monopile based on the bending moment profile, a 7th order polynomial is sufficient.
- At shallow depths the influence of scour type is more evident in the derived *p-y* curves, but becomes less significant as the depth increases. This indicates significant overburden dependency on the resistance properties of the soil, an effect which becomes lower for deeper depths.
- The distinction between *local* and *global* scour is not sufficient for determining the influence of scour type on *p-y* curves. The geometry of the local scour hole should also be considered as it highly affects the characteristics of the *p-y* curves in shallower soil layers. In the tests in this paper, a ≈20% reduction in ultimate *p-y* resistance was observed between local wide scour cases and local narrow scour cases. This therefore has ramifications for the lateral resistance properties of monopiles affected by local scour.
- An analysis that investigates the effect of scour formation on a rigid pile, should contain a series of scenarios with different scour geometries, as this parameter is crucial to the characteristics of the *p-y* curves. Note that since scour formation cannot yet be predicted accurately, it is still of importance to assess the influence of the various scour types for a given structure.

Future work will focus on appraising the performance of effective depths for scoured *p-y* curves for the geometrical cases considered in the present study. Effective depths can be used to appropriately modify *p-y* curves to account for scour presence. Furthermore, the additional resistance generated by laterally loaded rigid monopiles should be studied in more detail with a view to deriving simplified modelling parameters to incorporate the additional base stresses/moments and side shear resistances. These parameters could take the form of rotational springs distributed along the pile shaft to complement the lateral *p-y* curves. The use of *p-y* curves alone seems to be insufficient for capturing the lateral behavior of rigid monopiles.

Declaration of competing interest

The authors declare that they have no known competing financial interests or personal relationships that could have appeared to influence the work reported in this paper.

Acknowledgement

This work is partly funded by the Section of Geo-Engineering, Delft University of Technology and EU Horizon 2020 SAFE-10-T Project No. 723254. One author has been funded by the China Scholarship Council (CSC).

References

Achmus, M., 2010. Design of axially and laterally loaded piles for the support of offshore wind energy converters. Indian Geotech. Conf. 322–327.
Allersma, H.G.B., 1994. The University of Delft geotechnical centrifuge. Int. Conf. Centrifuge 94, 47–52.
API, 2007. RP2A: Recommended Practice for Planning, Designing and Constructing Offshore Platforms - Working Stress Design (Washington, DC).
ASTM, 2017. - 17 - Standard Practice for Classification of Soils for Engineering Purposes (Unified Soil Classification System) 10, p. D2487. https://doi.org/10.1520/D2487-17.
Bennett, C.R., Lin, C., Parsons, R., Han, J., 2009. Evaluation of behavior of a laterally loaded bridge pile group under scour conditions. In: Structures Congress 2009: Don't Mess with Structural Engineers: Expanding Our Role.
Brinkgreve, R.B.J., Kumarswamy, S., Swolfs, W., 2016. PLAXIS Manual (Delft, Netherlands).
Burd, H.J., Byrne, B.W., McAdam, R.A., Houlsby, G.T., Martin, C.M., JAP Beuckelaers, W., Zdravković, L., Taborda, D.M., Potts, D.M., Jardine, R.J., Gavin, K., Doherty, P., Igoe, D., Skov Gretlund, J., Pacheco Andrade, M., Muir Wood, A., 2017. Design aspects for monopile foundations. In: TC 209 Workshop on Foundation Design for Offshore Wind Structures,19th ICSMGE, pp. 35–44.
Byrne, B.W., Mcadam, R.A., Burd, H.J., Houlsby, G.T., Martin, C.M., Gavin, K., Doherty, P., Igoe, D., Zdravkovic, L., Taborda, D.M.G., Potts, D.M., Jardine, R.J., Sideri, M., Schroeder, F.C., Wood, A.M., Kallehave, D., Gretlund, J.S., 2015. Field testing of large diameter piles under lateral loading for offshore wind applications. In: Geotech. Eng. Infrastruct. Dev. - Proc. XVI Eur. Conf. Soil Mech. Geotech. Eng. ECSMGE, vol. 3, pp. 1255–1260, 2015.
Byrne, T., Gavin, K., Prendergast, L.J., Cachim, P., Doherty, P., Chenicheri Pulukul, S., 2018. Performance of CPT-based methods to assess monopile driveability in North Sea sands. Ocean Eng. 166, 76–91. https://doi.org/10.1016/j.oceaneng.2018.08.010.
Byrne, B.W., Burd, H.J., Gavin, K.G., Houlsby, G.T., Jardine, R.J., McAdam, R.A., Martin, C.M., Potts, D.M., Taborda, D.M.G., Zdravkovic, L., 2019. PISA: Recent Developments in Offshore Wind Turbine Monopile Design, pp. 350–355. https://doi.org/10.1007/978-981-13-2306-5_48.
De Jager, R.R., Maghsoudloo, A., Askarinejad, A., Molenkamp, F., 2017. Preliminary Results of Instrumented Laboratory Flow Slides. In: First International Conference on the Material Point Method. Elsevier Ltd, Delft, Netherlands.
Det Norske Veritas, 2007. Environmental Conditions and Environmental Loads, Recommended Practice DNV-RP-C205. https://doi.org/10.1109/INTLEC.1993.388591.
Doherty, P., Gavin, K., 2012. Laterally loaded monopile design for offshore wind farms. Proc. Inst. Civ. Eng. Energy 165, 7–17. https://doi.org/10.1680/ener.11.00003.
Dunnavant, T.W., 1986. Experimental and Analytical Investigation of the Behavior of Single Piles in Overconsolidated Clay Subjected to Cyclic Lateral Loads.
ENSOFT INC, 2018. LPILE.
Hajialilue-Bonab, M., Levacher, D., Chazelas, J.L., Kaynia, A.M., 2014. Experimental study on the dynamic behavior of laterally loaded single pile. Soil Dyn. Earthq. Eng. 66, 157–166. https://doi.org/10.1016/j.soildyn.2014.06.011.
Hoffmans, G.J., Verheij, H.J., 1997. Scour Manual. CRC Press.
Kampitsis, A.E., Sapountzakis, E.J., Giannakos, S.K., Gerolymos, N.a., 2013. Seismic soil–pile–structure kinematic and inertial interaction—a new beam approach. Soil Dyn. Earthq. Eng. 55, 211–224. https://doi.org/10.1016/j.soildyn.2013.09.023.
Kishore, Y.N., Rao, S.N., Mani, J.S., 2009. The behavior of laterally loaded piles subjected to scour in marine environment. KSCE J. Civ. Eng. 13, 403–408. https://doi.org/10.1007/s12205-009-0403-2.
LeBlanc, C., Houlsby, G.T., Byrne, B.W., 2010. Response of stiff piles in sand to long-term cyclic lateral loading. Geotechnique 60, 79–90. https://doi.org/10.1680/geot.7.00196.
Li, Y., Chen, X., Fan, S., Briaud, J., Chen, H.C., a, T., 2009. OTC 19906 is scour important for pile foundation design in Deepwater ?. In: Offshore Technology Conference https://doi.org/10.4043/19906-MS.
Li, F., Han, J., Lin, C., 2013. Effect of scour on the behavior of laterally loaded single piles in marine clay. Mar. Georesour. Geotechnol. 31, 271–289.
Li, Q., Prendergast, L.J., Askarinejad, A., Gavin, K.G., 2018. Effect of scour on the behavior of a combined loaded monopile in sand. In: 9th European Conference on Numerical Methods in Geotechnical Engineering. Porto, Portugal.
Liang, F., Zhang, H., Chen, S., 2018. Effect of vertical load on the lateral response of offshore piles considering scour-hole geometry and stress history in marine clay. Ocean Eng. 158, 64–77. https://doi.org/10.1016/j.oceaneng.2018.03.070.
Liang, F., Wang, C., Yu, X., 2019. Widths, types, and configurations: influences on scour behaviors of bridge foundations in non-cohesive soils (Bill). Mar. Georesour. Geotechnol. 37, 578–588. https://doi.org/10.1080/1064119X.2018.1460644.
Lin, C., Bennett, C., Han, J., Parsons, R.L., 2010. Scour effects on the response of laterally loaded piles considering stress history of sand. Comput. Geotech. 37, 1008–1014.
Matlock, H., 1970. Correlations for design of laterally loaded piles in soft clay. In: 2nd Annu. Offshore Technol. Conf., vol. 1, pp. 577–594. https://doi.org/10.4043/1204-MS.
Matutano, C., Negro, V., López-Gutiérrez, J.-S., Esteban, M.D., 2013. Scour prediction and scour protections in offshore wind farms. Renew. Energy 57, 358–365. https://doi.org/10.1016/j.renene.2013.01.048.
Mezazigh, S., Levacher, D., 1998. Laterally loaded piles in sand: slope effect on P-Y reaction curves. Can. Geotech. J. 35, 433–441. https://doi.org/10.1139/t98-016.
Mostafa, Y.E., 2012. Effect of local and global scour on lateral response of single piles in different soil conditions. Engineering 4, 297–306.

Murchison, J.M., O'Neill, M.W., 1984. Evaluation of p-y relationships in cohesionless soils. In: Analysis and Design of Pile Foundations. Proceedings of a Symposium in Conjunction with the ASCE National Convention, pp. 174–191.

Negro, V., López-Gutiérrez, J.-S., Esteban, M.D., Matutano, C., 2014. Uncertainties in the design of support structures and foundations for offshore wind turbines. Renew. Energy 63, 125–132. https://doi.org/10.1016/j.renene.2013.08.041.

Niemunis, A., Herle, I., 1997. Hypoplastic model for cohesionless soils with elastic strain range. Mech. Cohesive-Frict. Mater. 2, 279–299. https://doi.org/10.1002/(SICI)1099-1484 (199710)2:4<279::AID-CFM29>3.0.CO;2-8.

O'Neill, M., Murchinson, J.M., 1983. An Evaluation of P-Y Relationships in Sands.

Prakasha, K.S., Joer, H.A., Randolph, M.F., 2005. Establishing a model testing capability for deep water foundation systems. In: Front. Offshore Geotech. ISFOG 2005 - Proc. 1st Int. Symp. Front. Offshore Geotech., pp. 309–315.

Prendergast, L.J., Hester, D., Gavin, K., O'Sullivan, J.J., 2013. An investigation of the changes in the natural frequency of a pile affected by scour. J. Sound Vib. 332, 6685–6702. https://doi.org/10.1016/j.jsv.2013.08.020i.

Prendergast, L.J., Gavin, K., Doherty, P., 2015. An investigation into the effect of scour on the natural frequency of an offshore wind turbine. Ocean Eng. 101, 1–11. https://doi.org/10.1016/j.oceaneng.2015.04.017.

Prendergast, L.J., Reale, C., Gavin, K., 2018. Probabilistic examination of the change in eigenfrequencies of an offshore wind turbine under progressive scour incorporating soil spatial variability. Mar. Struct. 57, 87–104. https://doi.org/10.1016/j.marstruc.2017.09.009.

Qi, W., Gao, F., 2014. Equilibrium scour depth at offshore monopile foundation in combined waves and current. Sci. China Technol. Sci. 57, 1030–1039. https://doi.org/10.1007/s11431-014-5538-9.

Qi, W.G., Gao, F.P., Randolph, M.F., Lehane, B.M., 2016. Scour effects on *p–y* curves for shallowly embedded piles in sand. Geotechnique 66, 648–660. https://doi.org/10.1680/jgeot.15.P.157.

Reese, L., Welch, R.C., 1975. Lateral loadings of deep foundations in stiff clay. J. Geotech. Eng. 101, 633–649.

Reese, L.C., Cox, W.R., Koop, F.D., 1974. Analysis of laterally loaded pilesin sand. In: 6th Annual Offshore Technology Conf, pp. 473–484.

Reese, L.C., Cox, W.R., Koop, F.D., 1975. Field testing and analysis of laterally loaded piles in stiff clay. In: Proceedings, 7th Offshore Technology Conference, pp. 671–690. https://doi.org/10.4043/2312-MS.

Reese, L.C., Wang, S., Long, J., 1989. Scour from cyclic lateral loading of piles. Offshore Technol. Conf. https://doi.org/10.4043/6005-MS.

Remaud, D., 1999. Pieux sous charges latérales: étude expérimentale de l'effet de groupe. Confrontation.

Roulund, A., Sumer, B.M., Michelsen, J., 2005. Numerical and experimental investigation of flow and scour around a circular pile. J. Fluid Mech. 534, 351–401. https://doi.org/10.1017/S0022112005004507.

Peder Hyldal Sørensen, S., Bo Ibsen, L., 2013. Assessment of foundation design for offshore monopiles unprotected against scour. Ocean Eng. 63, 17–25. https://doi.org/10.1016/j.oceaneng.2013.01.016.

Sumer, B.M., Fredsøe, J., 2012. The mechanics of scour in the marine environment. Adv. Ser. Ocean Eng. 17.

von Wolffersdorff, P.-A., 1996. Hypoplastic relation for granular materials with a predefined limit state surface. Mech. Cohesive-Frict. Mater. 1, 251–271. https://doi.org/10.1002/(SICI)1099-1484(199607)1:3<251::AID-CFM13>3.0.CO;2-3.

Wang, J., Qi, C., 2008. P-y curves of piles in saturated degradation sands with residual pore water pressures. Isope 8, 690–697.

Wang, S.T., Reese, L.C., 1991. "Analysis of Piles under Lateral Load-Computer Program COM624P for the microcomputers." Report No. FHwA-SA-91-002. U.S. Dept. of Transportation, FHwA, Washington, D.C.

Wilson, D.W., 1998. Soil-pile-superstructure interaction in liquefying sand and soft clay. Transp. Res. Rec. 1569, 190. https://doi.org/10.3141/1569-07.

Wind Europe, 2018. Offshore wind in Europe - key trends and statistics. Refocus 3, 14–17. https://doi.org/10.1016/S1471-0846(02)80021-X.

Xue, J., Gavin, K., Murphy, G., Doherty, P., Igoe, D., 2016. Optimization technique to determine the p-y curves of laterally loaded stiff piles in dense sand. Geotech. Test J. 39, 842–854. https://doi.org/10.1520/GTJ20140257.

Yang, K., Liang, R., 2007. Methods for deriving p-y curves from instrumented lateral load tests. Geotech. Test J. 30, 31–38.

Yankelevsky, D.Z., Eisenberger, M., Adin, M.A., 1989. Analysis of beams on nonlinear winkler foundation. Comput. Struct. 31, 287–292. https://doi.org/10.1016/0045-7949(89)90232-0.